SUPPLEMENTARY MATERIALS

Materials and Methods

Supplemental Figures 1 to 17

Supplemental Materials and Methods

Retrospective cohort Study

The complete retrospective cohort contained females with a median age of 49 years at diagnosis (23–80 years old). Of these patients, 11.1% were 35 years of age or under, 54.1% were premenopausal, and 41.2% had lymph node metastasis at the time of surgery. Primary therapy was based on patient condition and in accordance with National Comprehensive Cancer Network. Treatment consisted of surgical resection along with adjuvant therapy (hormone, chemotherapy, and radiation). Baseline patient characteristics and treatment outcomes (overall survival [OS], disease-free survival [DFS]) were collected from medical records, medical appointments, or by telephone. DFS (primary endpoint) was defined as the time from surgery to breast cancer relapse, including clinical relapse with histopathological or radiological confirmation, a second cancer, or death. OS (secondary endpoint) was the time from surgery to death by any cause. The clinical information, including follow-up information for most cases, was included in our previous studies (1).

IHC scoring was performed in a blinded fashion by two independent pathologists using the immunoreactive score (IRS) proposed by Remele and Stegner. An IRS of no less than 3 points was classified as positive expression.

Serum and organ collection and pathological analysis

Submandibular blood collection was performed for the preparation of serum. The blood was collected in BD gold top vacutainer tubes. After standing at room temperature for 20–30 min for clot formation, the samples were centrifuged at 15°C for 10 min at 5000 rpm. The serum was transferred to precooled vials and stored at -80°C. A complete biochemical panel was performed on the serum samples at the Comparative Pathology & Mouse Phenotyping Shared Resource of OSU. Mice were euthanized by carbon dioxide inhalation, and abdominal skin, lung, heart, liver, kidney, spleen, and gastrointestinal tract were collected. Each organ was weighed and then fixed in 10% formalin at room temperature for 72 h. Histological processing was performed by the Comparative Pathology & Mouse Phenotyping Shared Resource of OSU. For hematoxylin and eosin (H&E) staining, followed by dehydration in degraded ethanol, immersion in xylene, and mounting in Permount medium. The slides were analyzed by the Comparative Pathology & Digital Imaging Shared Resource, Department of Veterinary Biosciences and the Comprehensive Cancer Center of OSU.

G2/M phase checkpoint

Cell cycle distribution was determined by flow cytometry. Cells were centrifuged, resuspended in phosphate-buffered saline (PBS), fixed with 70% ice-cold ethanol, and stored at 4ºC overnight. After washing three times with cold PBS, the cell suspension was incubated with DNase-free RNase (100 μg/mL; Sigma-Aldrich) at 37ºC for 30 min. After fixation, the cells were co-stained with propidium iodide and anti-phospho-Histone H3 (pS10)-specific antibody conjugated with Alexa Fluor 488 (Cell Signaling Technology, Danvers, MA, USA). Samples

were analyzed (15,000 events per sample) using the FACScan flow cytometer (BD Pharmingen, San Diego, CA, USA).

Cycloheximide assay

Cells (6×10^5) were seeded in 60-mm culture dishes and incubated overnight in a CO_2 incubator. The medium was replaced with cycloheximide (CHX; 100 µg/mL in DMSO)-containing medium Cell samples were collected for western blotting at various time points.

Reactive oxygen species detection

Reactive oxygen species (ROS) assay was performed with the DCFDA/H2DCFDA-Cellular ROS Assay Kit (ab113851, Cat No. GR3313162-11, Abcam) following the manufacturer's instructions. H_2O_2 as the positive control and measure fluorescence on the microplate reader Synergy H1 (BioTek)

Squalene and cholesterol detection by liquid chromatography-mass spectrometry (LC-MS)

The cells were extracted with methanol, dried using a SpeedVac, and re-extracted with 400 µL of chloroform:methanol (2:1) containing 1 ppm of heavy-labeled 5C13-cholesterol. The extracts were sonicated for 30 min and washed with 200 µL water followed by centrifugation. The organic layer (200 µL) was transferred into a clean tube and dried. The samples were resuspended in 50 µL of acetonitrile containing 0.05% formic acid. Squalene and cholesterol calibration solutions (0.0, 0.025, 0.1, 0.25, 1.0, 5.0, 25.0, 100, and 200 µg/mL) were made by diluting stocks of each in

chloroform:methanol (2:1) solution with heavy-labeled cholesterol and processing them exactly as the cell extracts. The samples were quantified using an atmospheric chemical ionization source (APCI) on a Thermo Scientific TQS Quantiva triple quadrupole mass spectrometer, and separation was achieved using a Thermo Scientific Ultimate 3000 HPLC with an Agilent Poroshell 120 SB-C18 (2x100 mm, 2.7 µm particle size) reverse-phase column. Samples (3 µL) were separated at a flow rate of 300 µL/min with an isocratic gradient of 98% H_2O with 0.1% formic acid and 2% 80:20 ACN: IPA with 0.1% formic acid. The APCI ion source was held at a 5 µA discharge current in positive mode with a sheath gas of 45, ion transfer tube of 300°C, and a vaporizer temp of 350°C. For squalene (RT 4.34 min), the transitions monitored were the precursor 411.5 m/z and product ions 149.1 and 231.1 m/z at collision energies of 21 and 18 V, respectively. Cholesterol (RT 3.49 min) was monitored at the precursor 369.4 m/z and product ions 147.1 and 161.1 m/z at collision energies of 21 and 19 V, while the internal standard 5C13-cholesterol (RT 3.49 min) was monitored from 374.4 m/z to product ions 135.1 and 147.1 m/z at collision energies of 21 and 23 V.

Cholesterol measurements

Cells were centrifuged at 1,000 rpm for 10 min, and the pellets resuspended in 1% Triton X-100 in isopropanol for 1 h at room temperature. The samples were centrifuged for 10 min at 12,000 rpm. The supernatants were dried under nitrogen, and the cholesterol levels were measured with the Amplex™ Red Cholesterol Assay Kit (Cat No. A12216, Invitrogen), following the manufacturer's instructions.

Real-time quantitative reverse transcription PCR

Real-time quantitative reverse transcription-PCR (qRT-PCR) was performedto determine the mRNA levels (2,3). The primers used for qRT-PCR were below:

Gene	Direction	5’ to 3’
SQLE	R	GGCATCAAGACCTTCCACTG
	F	GCTGTGCTTTCCAGAGATGG
Wip1	R	CAAGATTGTCCATGCTCACC
	F	GGGAGTGATGGACTTTGGAA
GRP78	R	TTCTGCTGTATCCTCTTCACCAGT
	F	TGTTCAACCAATTATCAGCAAACTC
ATF4	R	ATCCTGCTTGCTGTTGTTGG
	F	GTTCTCCAGCGACAAGGCTA
CHOP	R	TCTCCTTCATGCGCTGCTTT
	F	AGAACCAGGAAACGGAAACAGA
sXBP1	R	ATCCATGGGGAGATGTTCTGG
	F	CTGAGTCCGAATCAGGTGCAG
GAPDH	R	TTAAAAGCAGCCCTGGTGAC
	F	CTCTGCTCCTCCTGTTCGAC

Western blotting

Western blotting was performed as previously described (2,4). The primary antibody against SQLE (12544-1-AP, 1:1000) was obtained from Proteintech, and the anti-phospho-RPA32 Ser33 antibody (A300-246A, 1:1,000) was from Bethyl Laboratories. The antibodies against RPA2 (Clone NA18, 1:100), β-actin (Clone AC-74, 1:50000), and phospho-histone H2AX Ser139 (clone JBW301, 1:1000) were purchased from MilliporeSigma. The antibodies against histone H2AX (D17A3, 7631, 1:1000), phospho-ATM Ser1981 (10H11.E12, 4526, 1:500), ATM (D2E2, 2873,

1:1000), BiP (C50B12, 3177, 1:1000) phospho-eIF2α (Ser51, 9721, 1:1000) and eIF2α (9722, 1:1000), and secondary antibodies goat-anti-mouse IgG-horseradish peroxidase (HRP) (7076S, 1:3000) and goat-anti-rabbit IgG-HRP (7074S, 1:3000) were obtained from Cell Signaling Technology. The antibody against WIP1 (F-10, sc-376257, 1:1000) and the donkey anti-goat IgG–HRP conjugated secondary antibody (A2216, 1:3000) were from Santa Cruz Technology.

Immunofluorescence

Immunofluorescence was conducted as described previously (3,4) . The primary antibodies used were against: phospho-histone H2A.X ser139 (clone JBW301, 1:400, MilliporeSigma); p-RPA32 (S33, A300-246A, 1:400, Bethyl Laboratories); ATM protein kinase S1981 (200-301-400, 1:100, Rockland); RAD51 (sc-8349, 1:50, Santa Cruz Biotechnology). The goat anti-mouse IgG (H+L) Alexa Fluor 594 (A-11032, 1:400,) and chicken anti-rabbit IgG (H+L) Alexa Fluor 488 (A-21441, 1:400) secondary antibodies were from Thermo Fisher Scientific. Images were collected at 63× oil magnification using a Zeiss Axio Observer inverted fluorescence microscope (X-Cite 120LED).

Lipid droplet staining and quantification

Cells were treated with SQLE inhibitors for 24 h. The LDs in live cells were stained with 0.5 μM BODIPY 493/503 (D-3922, Thermo Fisher Scientific) for 30 min, and the nuclei were then counterstained with 5 μg/mL Hoechst 33342 (H3570, Life Technologies) for 30 min. Staining was visualized by confocal microscopy (Carl Zeiss LSM510 Meta or LSM800, 63× /1.4 NA oil, 1 μM-wide z-stack). Staining ($n \geq 30$ cells per group) was quantified using ImageJ software (NIH) in a 3D stack, as described previously (5).

Flow cytometry (FACS)

Cell cycle analysis was performed as described previously (25). Apoptosis was measured using the Annexin V-FITC Early Apoptosis Detection Kit (cat. 6592, Cell Signaling Technology), following the manufacturer's instructions. Combined inhibition of Aurora kinase inhibitor Alisertib (MLN8237, cat. No. S1133, Selleckchem Company) and BCL inhibitor Navitoclax (ABT-263, cat. No. S1001, Selleckchem Company) were used as positive control.

Supplemental Figs. S1 to S17

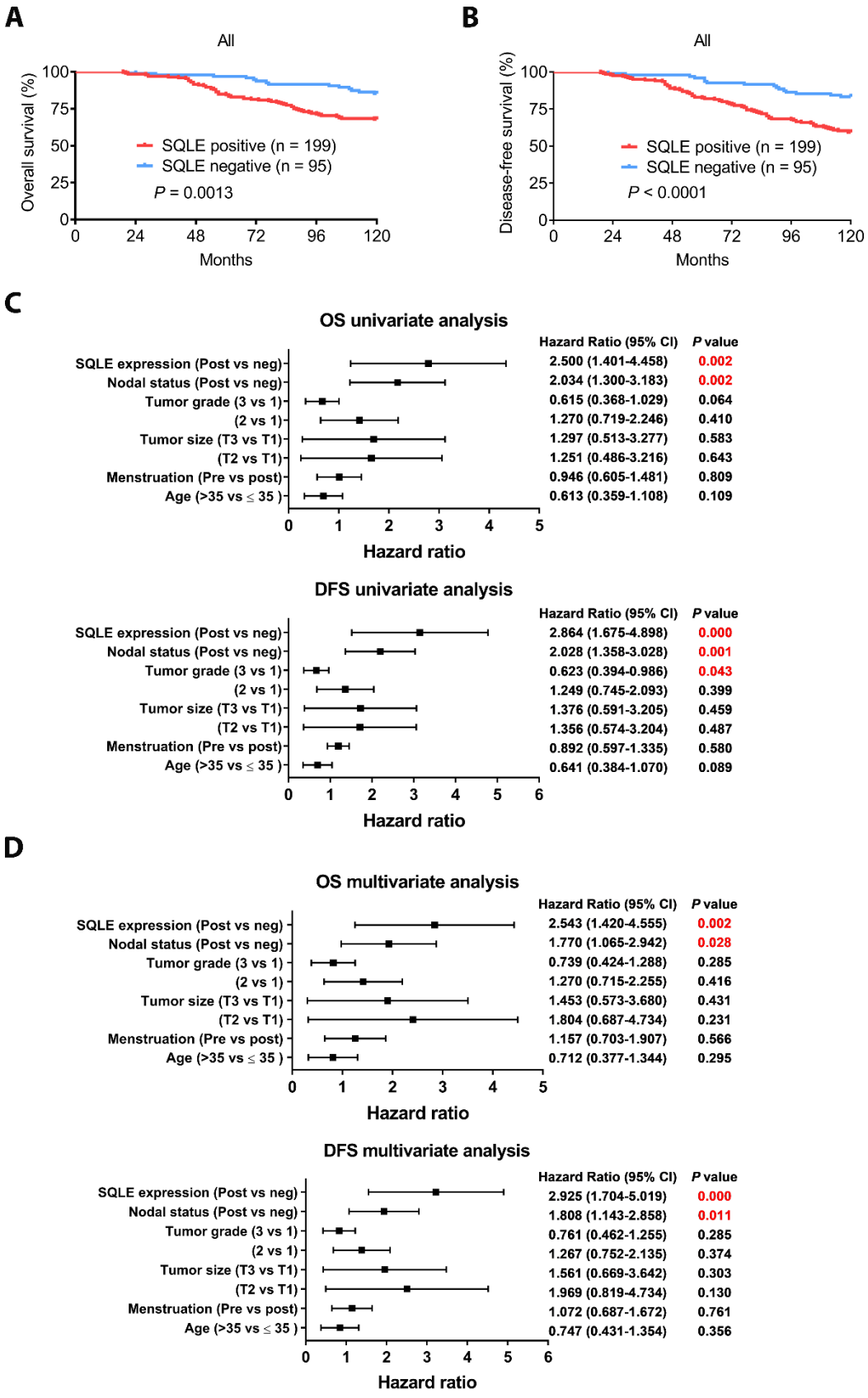
A
All
Overall survival (%)
100
75
50
25
0
0
24
48
72
96
120
Months
SQLE positive (n = 199)
SQLE negative (n = 95)
P = 0.0013
B
All
Disease-free survival (%)
100
75
50
25
0
0
24
48
72
96
120
Months
SQLE positive (n = 199)
SQLE negative (n = 95)
P < 0.0001
C
OS univariate analysis
Hazard Ratio (95% CI)
P value
SQLE expression (Post vs neg)
2.500 (1.401-4.458)
0.002
Nodal status (Post vs neg)
2.034 (1.300-3.183)
0.002
Tumor grade (3 vs 1)
0.615 (0.368-1.029)
0.064
(2 vs 1)
1.270 (0.719-2.246)
0.410
Tumor size (T3 vs T1)
1.297 (0.513-3.277)
0.583
(T2 vs T1)
1.251 (0.486-3.216)
0.643
Menstruation (Pre vs post)
0.946 (0.605-1.481)
0.809
Age (>35 vs ≤ 35)
0.613 (0.359-1.108)
0.109
0
1
2
3
4
5
Hazard ratio
DFS univariate analysis
Hazard Ratio (95% CI)
P value
SQLE expression (Post vs neg)
2.864 (1.675-4.898)
0.000
Nodal status (Post vs neg)
2.028 (1.358-3.028)
0.001
Tumor grade (3 vs 1)
0.623 (0.394-0.986)
0.043
(2 vs 1)
1.249 (0.745-2.093)
0.399
Tumor size (T3 vs T1)
1.376 (0.591-3.205)
0.459
(T2 vs T1)
1.356 (0.574-3.204)
0.487
Menstruation (Pre vs post)
0.892 (0.597-1.335)
0.580
Age (>35 vs ≤ 35)
0.641 (0.384-1.070)
0.089
0
1
2
3
4
5
6
Hazard ratio
D
OS multivariate analysis
Hazard Ratio (95% CI)
P value
SQLE expression (Post vs neg)
2.543 (1.420-4.555)
0.002
Nodal status (Post vs neg)
1.770 (1.065-2.942)
0.028
Tumor grade (3 vs 1)
0.739 (0.424-1.288)
0.285
(2 vs 1)
1.270 (0.715-2.255)
0.416
Tumor size (T3 vs T1)
1.453 (0.573-3.680)
0.431
(T2 vs T1)
1.804 (0.687-4.734)
0.231
Menstruation (Pre vs post)
1.157 (0.703-1.907)
0.566
Age (>35 vs ≤ 35)
0.712 (0.377-1.344)
0.295
0
1
2
3
4
5
Hazard ratio
DFS multivariate analysis
Hazard Ratio (95% CI)
P value
SQLE expression (Post vs neg)
2.925 (1.704-5.019)
0.000
Nodal status (Post vs neg)
1.808 (1.143-2.858)
0.011
Tumor grade (3 vs 1)
0.761 (0.462-1.255)
0.285
(2 vs 1)
1.267 (0.752-2.135)
0.374
Tumor size (T3 vs T1)
1.561 (0.669-3.642)
0.303
(T2 vs T1)
1.969 (0.819-4.734)
0.130
Menstruation (Pre vs post)
1.072 (0.687-1.672)
0.761
Age (>35 vs ≤ 35)
0.747 (0.431-1.354)
0.356
0
1
2
3
4
5
6
Hazard ratio

Supplemental Figure S1. SQLE expression correlated with poor survival and predicted patient outcome. A and **B,** BC patients with positive SQLE staining had a low overall survival rate and worse 5-year DFS than those with negative SQLE staining. **C,** Cox regression of univariate analysis of OS and DFS in BC cohorts. **D,** Cox regression of multivariate analysis of OS and DFS in BC cohorts. Survival in **A** and **B** were determined using the Kaplan-Meier method, and differences between groups were tested using the log-rank test. Univariate and multivariate analyses in **C** and **D** were performed with the cox proportional hazard regression model.

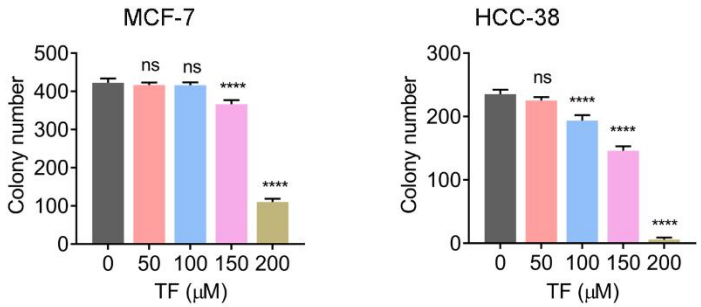

Supplemental Figure S2. Colony formation by breast cancer cells following SQLE inhibition with terbinafine (TF). A TF dose of 50 μM did not significantly inhibit cell viability and was used for further assays. Data are presented as the mean ± SD. Statistical significance was determined by one-way ANOVA versus the control. ****, $P < 0.0001$; ns, not significant.

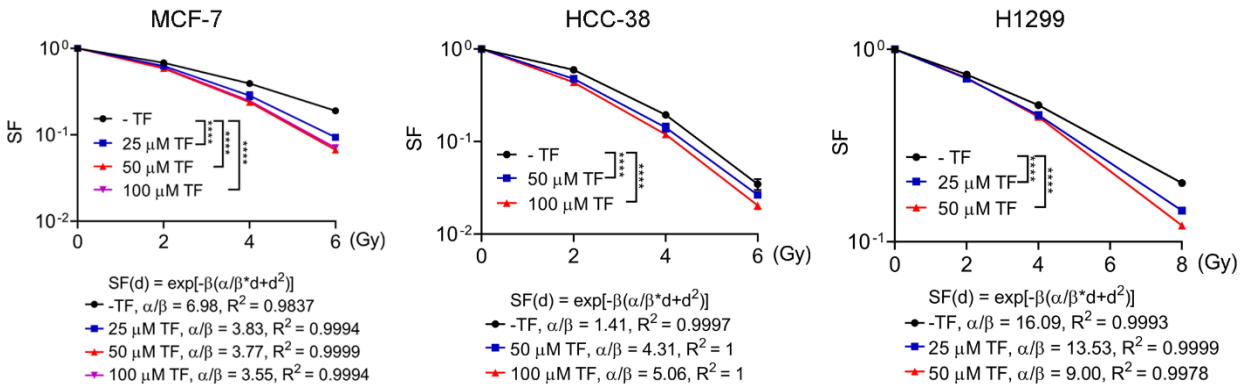

Supplemental Figure S3. Extraction of α/β values for Fig. 2B survival curves using the linear-quadratic (LQ) model. R^2 coefficients close to 1 for each fitting indicated that the regression predictions almost perfectly fitted the data. The α/β values extracted for the breast (MCF-7 and HCC-38) and lung (H1299) cancer lines were consistent with the conventional consensus of $\alpha/\beta \approx 4$ for breast cancer and $\alpha/\beta \approx 10$ for lung cancer in the field of radiation therapy **(6,7)**. SQLE inhibition decreased the α/β values in these cell lines, suggesting increased radiosensitivity. TF was given 24 h prior to irradiation. Data are presented as the mean ± SD. Statistical significance in each group was evaluated by two-way ANOVA and the Bonferroni post-hoc test. ****, $P < 0.0001$.

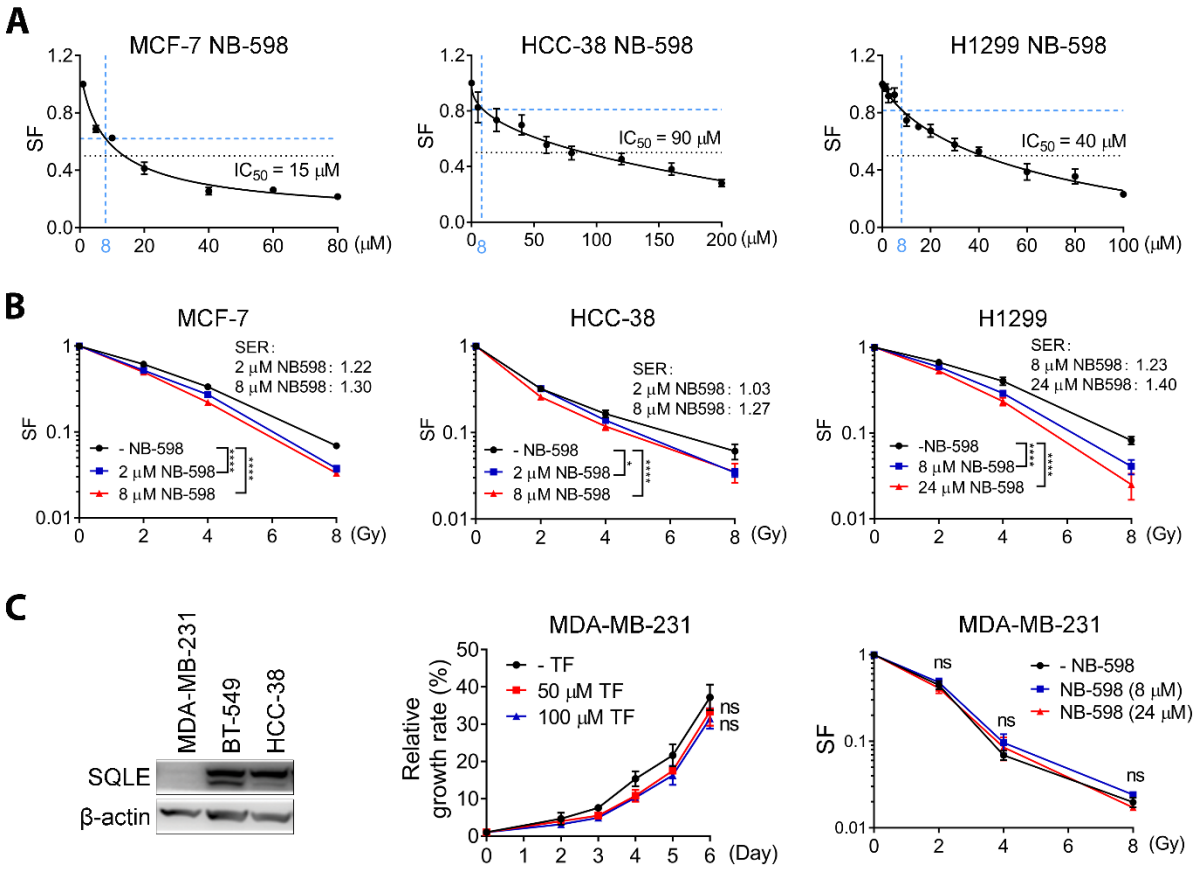

Supplemental Figure S4. SQLE inhibition enhanced IR sensitivity *in vitro* and *in vivo*. A, The IC_{50}s of NB-598 in MCF-7, HCC-38 and H1299 cancer cells. Blue dash lines indicate the non-toxic dose of NB-598 that was used for the colony formation assay (8 μM NB-598). **B,** *In vitro* colony formation assay showed SQLE inhibition by NB-598 sensitized BC and NSCLC cells to IR. (SER, Sensitizer enhanced ratio). **C,** SQLE inhibited by 50 μM TF or 8 μM NB-598 had no impact on BC cells with undetectable SQLE (MDA-MB-231). Data in **B** and **C** are presented as mean ± SD. Statistical significance was evaluated by one-way (**C**, left) or two-way (**B**; **C**, right) ANOVA and the Bonferroni post-hoc test. **, $P < 0.01$; ***, $P < 0.001$; ****, $P < 0.0001$; ns, not significant.

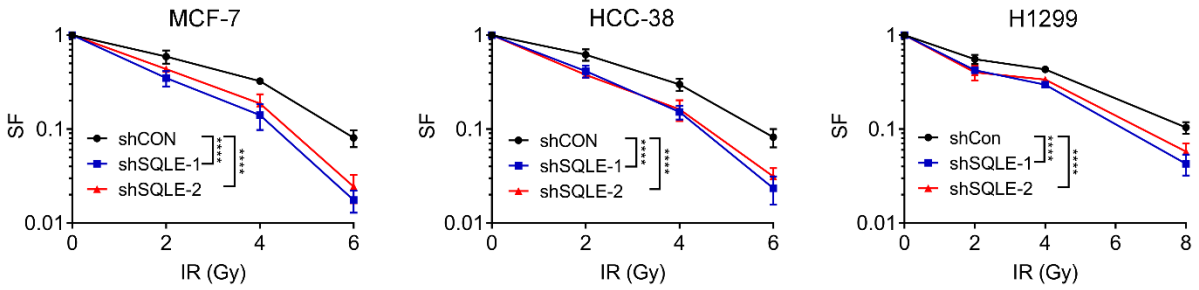

Supplemental Figure S5. SQLE inhibition by shRNA enhanced the radiosensitivity of breast and lung cancer cell lines. Radiosensitivity was determined using the colony formation assay. Data are presented as the mean ± SD. Statistical significance was evaluated by two-way ANOVA and the Bonferroni post-hoc test. ****, $P < 0.0001$.

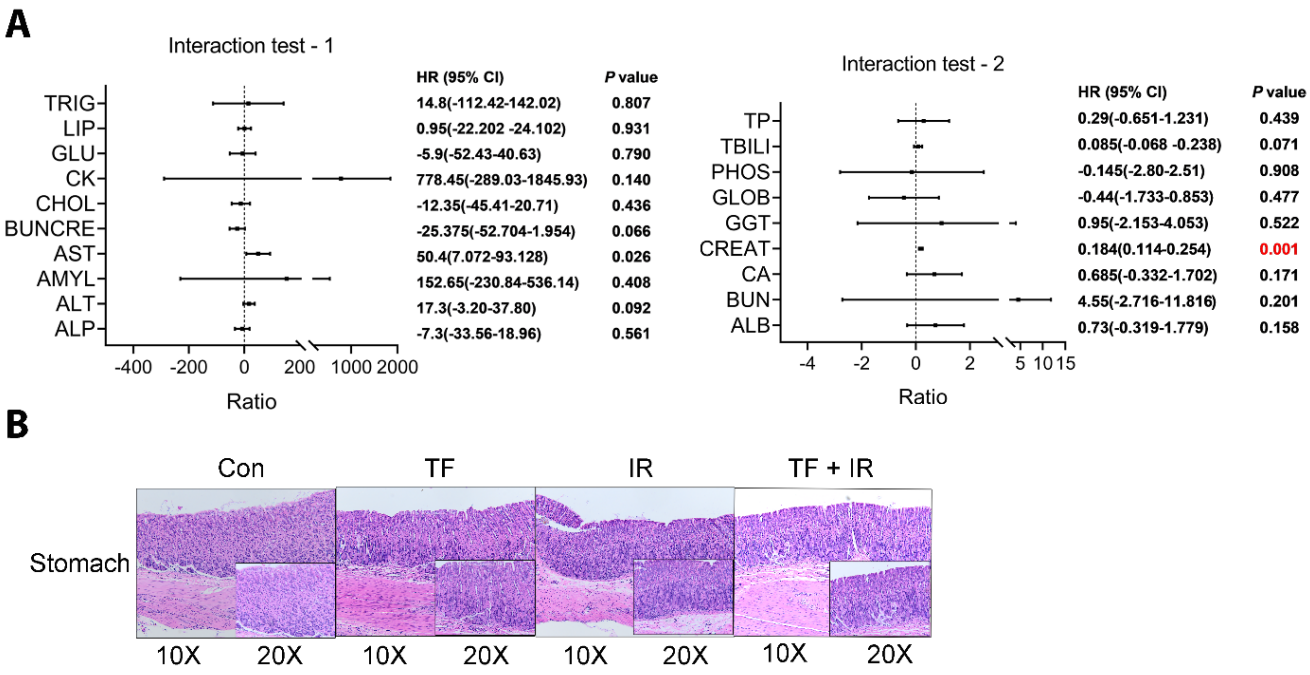

Supplemental Figure S6. Analysis of serum biochemistry profiling and histological detection indicated no toxicity in combination of TF and RT. A, Interaction test showed all serum parameters were not significantly changed in the TF-treated or TF combined with IR groups. Although CREAT indicated statistically significant changes ($P < 0.001$), the CREAT values of each group were still in the normal range. Cox proportional hazard regression model was performed. TRIG, triglyceride; LIP, lipase; GLU, glucose; CK, creatinine kinase; CHOL, cholesterol; BUNCRE, the ratio of BUN to CREAT; AST, aspartate aminotransferase; AMYL, amylase; ALT, alanine aminotransferase; ALP, alkaline phosphatase; TP, total protein; TBLI, total bilirubin; PHOS, phosphorus; GLOB, globulins; GGT, gamma-glutamyl transferase; CREAT, creatinine; CA, calcium; BUN, blood urea nitrogen; ALB, albumin. **B,** Representative histological images of the stomach from the four treatment groups showed insignificant lesions in the TF-treated or TF combined IR groups (magnification, 10× and 20×).

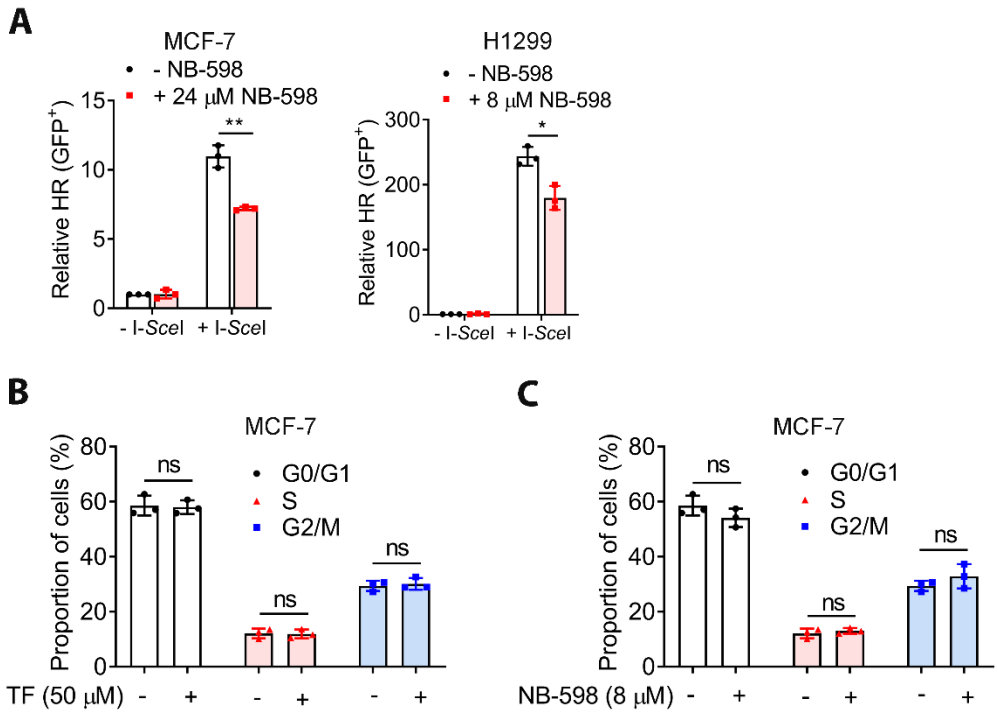

Supplemental Figure S7. SQLE inhibition impaired HR. A, SQLE inhibition impaired HR. The percentage of I-*Sce*I-induced GFP-positive cells was significantly decreased in NB-598-treated MCF-7 and H1299 cells. All data are normalized with Con group. **B** and **C,** The effect of SQLE inhibitors on the cell cycle of MCF-7 cells. Statistical significance was determined by one-way ANOVA followed by Bonferroni's post-hoc analysis for multiple comparisons. *, $P < 0.05$; **, $P < 0.01$; ns, not significant.

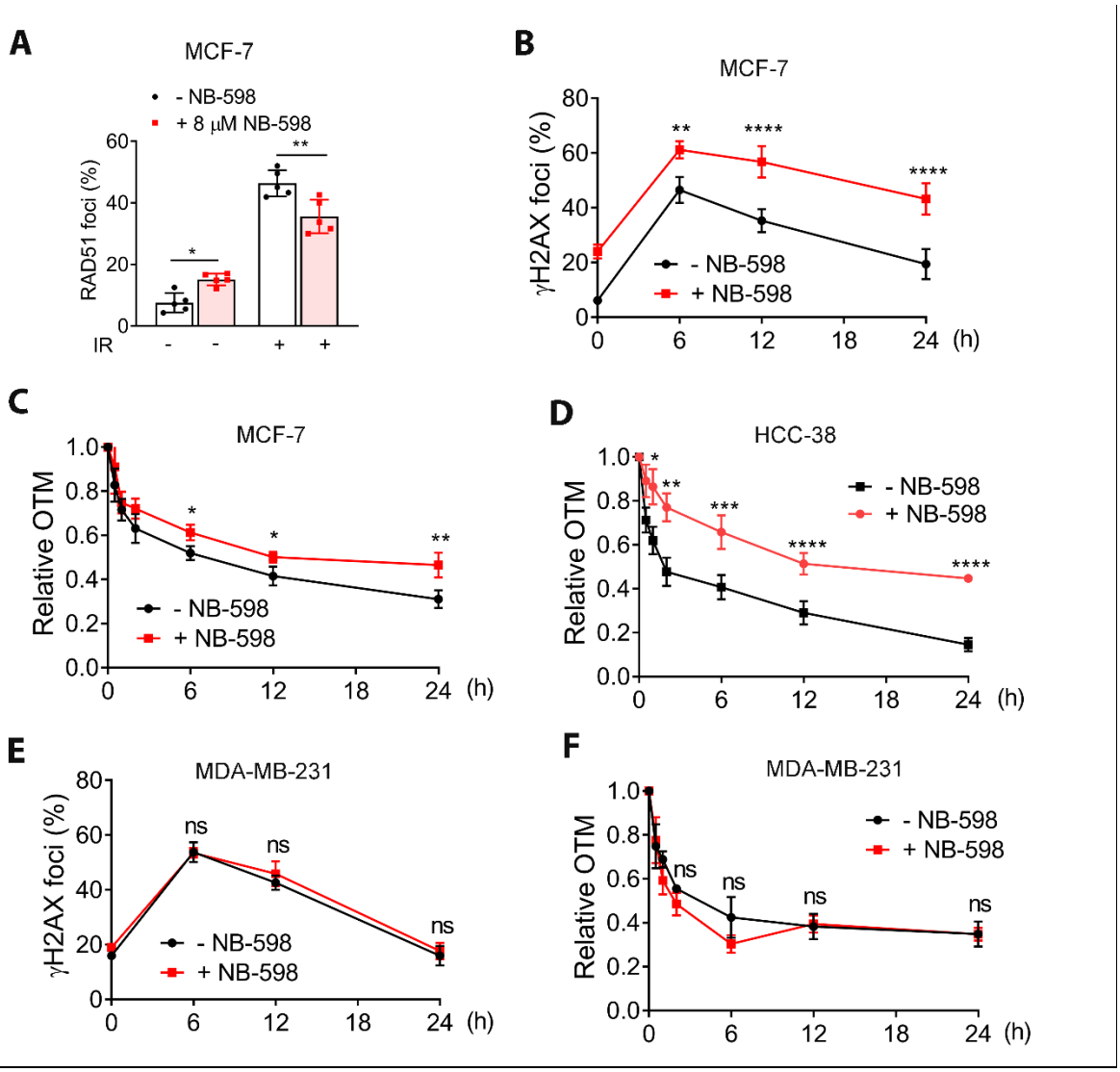

Supplemental Figure S8. SQLE inhibition impaired HR activity and delayed RT-induced DSB repair in SQLE expression cells. A, SQLE inhibition by NB-598 abrogated IR-induced RAD51 foci formation, as detected by the immunostaining of MCF-7 cells. **B,** Accumulated DSBs were observed in MCF-7 cells treated with 8 μM NB-598, as detected by γH2AX foci staining. **C** and **D,** SQLE inhibition by 8 μM NB-598 lead to DSB accumulation, as detected by the comet assay. OTM, olive tail moment. SQLE inhibition by 8 μM NB-598 promoted IR-induced DSBs in MCF-7 and HCC-38 cells. **E** and **F,** SQLE inhibition had no impact on IR-induced DSB repair in MDA-MB-231 cells, as detected by immunostaining and comet assay. Data are presented as the mean ± SD. Statistical significance was determined by one-way (**A**) or two-way (**B** to **F**) ANOVA followed by Bonferroni's post-hoc analysis for multiple comparisons. *, $P < 0.05$; **, $P < 0.01$; ***, $P < 0.001$; ****, $P < 0.0001$; ns, not significant.

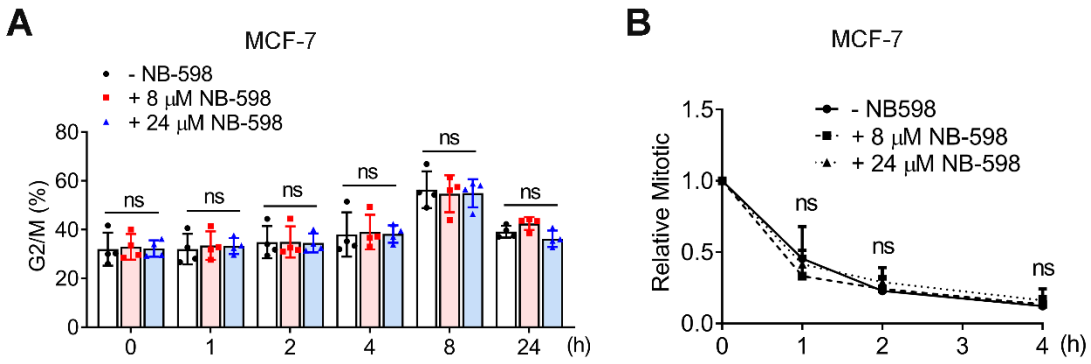

Supplemental Figure S9. SQLE inhibitor had no effect on IR-induced G2/M checkpoints. A, The percentage of total cells in the G2/M phase after SQLE inhibition in MCF-7 cells. G2/M accumulation at different time-points post-8 Gy IR was detected with propidium iodide by flow cytometry. **B,** SQLE inhibition had no effect on the mitotic ratio in MCF-7 cells following IR (IR, 8 Gy). Phosphor-histone H3-Ser10 staining was used to calculate the mitotic ratio. All data are presented as the mean ± SEM from triplicate experiments. Statistical significance was evaluated by one-way ANOVA and Bonferroni's post-hoc test. Ns, not significant.

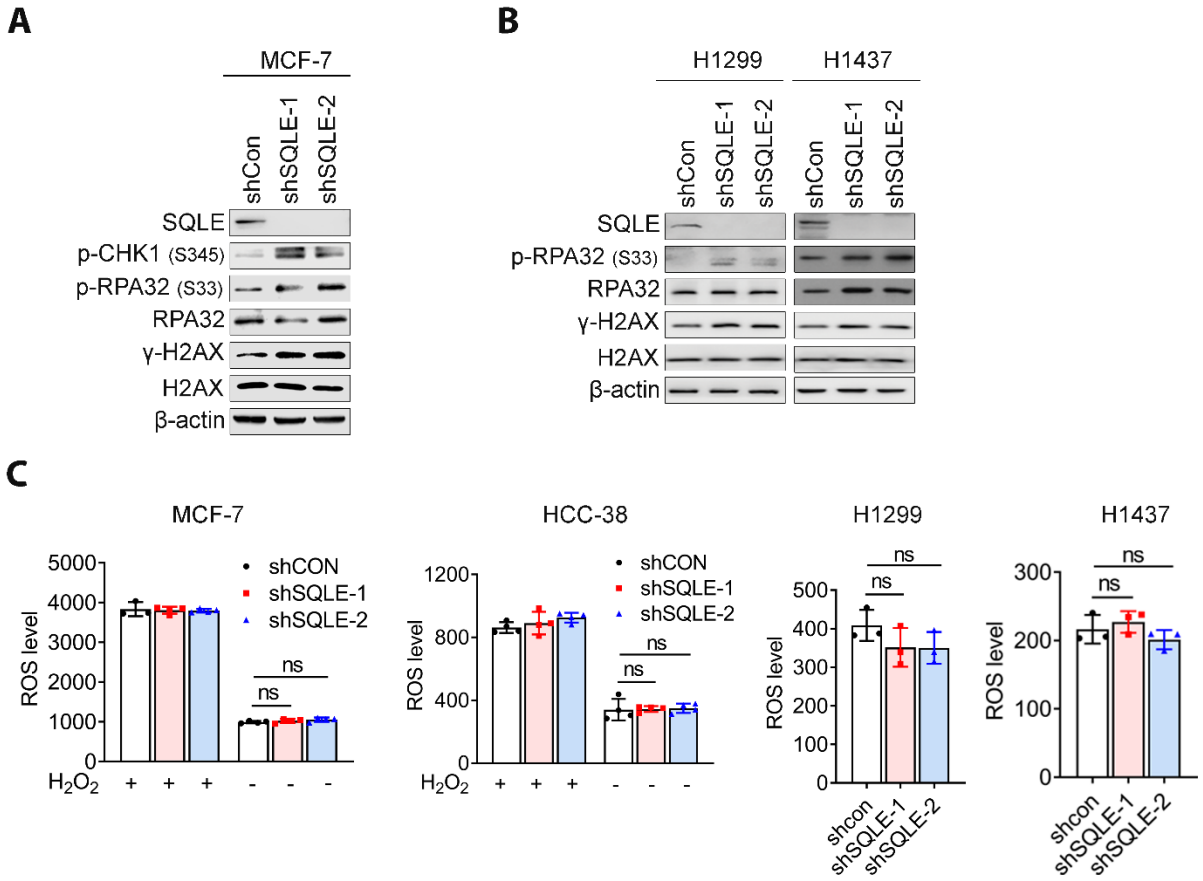

Supplemental Figure S10. SQLE inhibition increased RS but had no impact on ROS levels. **A** and **B,** SQLE inhibited by shRNA knockdown or inhibitor increased RS in BC and lung cancer cells, as detected by RS markers. **C,** The ROS levels were similar in BC and lung cancer cells with or without SQLE knockdown. ROS were detected using a fluorogenic dye (DCFDA/H2DCFDA). Data are presented as the mean ± SD. Statistical significance was evaluated with one-way ANOVA and Bonferroni's post-hoc test. Ns, not significant.

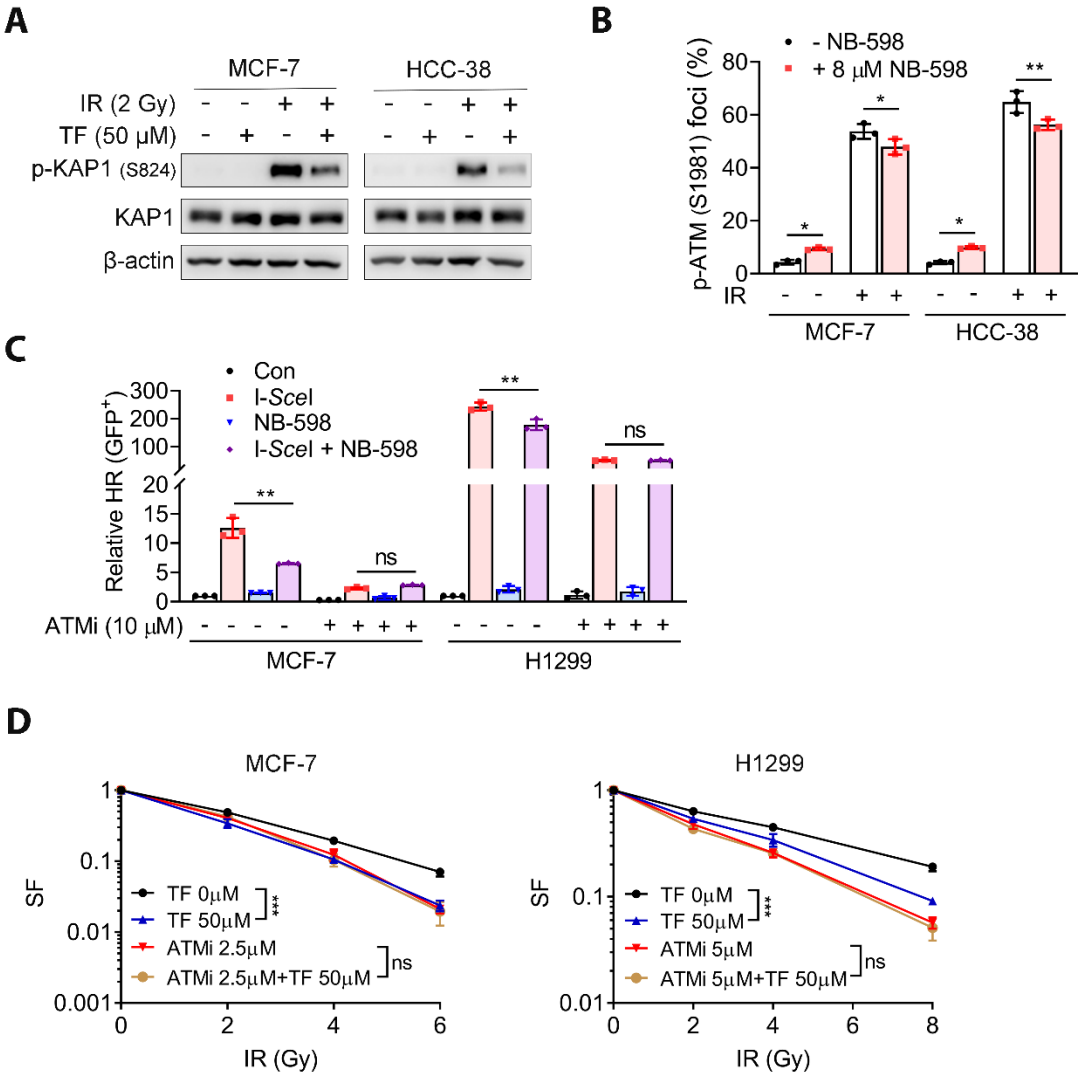

Supplemental Figure S11. SQLE inhibition impaired ATM activity. A. SQLE inhibition reduced IR-induced p-KAP1. **B,** SQLE inhibition decreased IR-induced p-ATM (S1981) foci in MCF-7 and HCC-38 cells detected by immunofluorescence staining (30 min post 2 Gy IR). Data are presented as the mean ± SD. **C,** ATM inhibition abrogated the reduction in HR caused by 8 μM NB-598 in MCF-7 and H1299 cells, as detected using the HR-DrGFP reporter. All data in **C** are normalized with Con group. **D.** ATM inhibition abrogates TF-induced radio sensitivity. TF was given 24 h prior to irradiation (**D**). Data are presented as the mean ± SD. Statistical significance was evaluated with one-way (**B** and **C**) or two-way (**D**) ANOVA and Bonferroni's post-hoc test. *, $P < 0.05$; **, $P < 0.01$; ***, $P < 0.001$; ns, not significant.

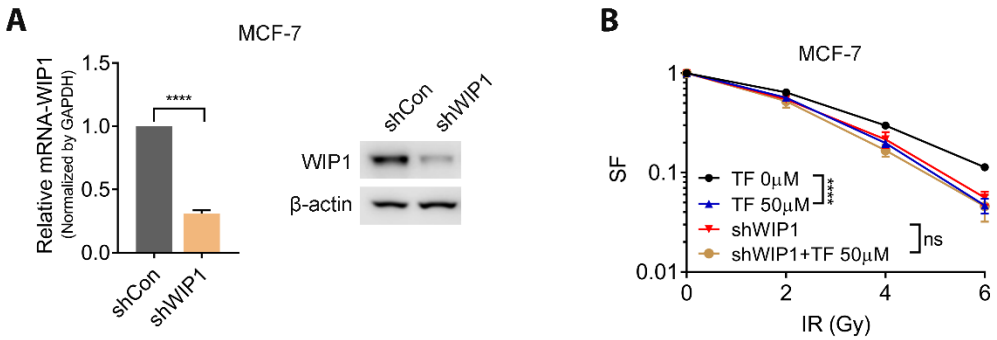

Supplemental Figure S12. WIP1 knockdown abrogated SQLE inhibition-induced radiosensitivity. **A**, WIP1 knockdown by shRNA (shWIP1) was validated by RT-PCR and WB. **B**, WIP1 knockdown eliminated TF-induced radiosensitivity in MCF-7 cells. Data are presented as the mean ± SD. TF was given 24 h prior to irradiation (**B**). Statistical significance was evaluated with the t-test (**A**) or two-way (**D**) ANOVA and Bonferroni's post-hoc test. ****, $P < 0.0001$; ns, not significant.

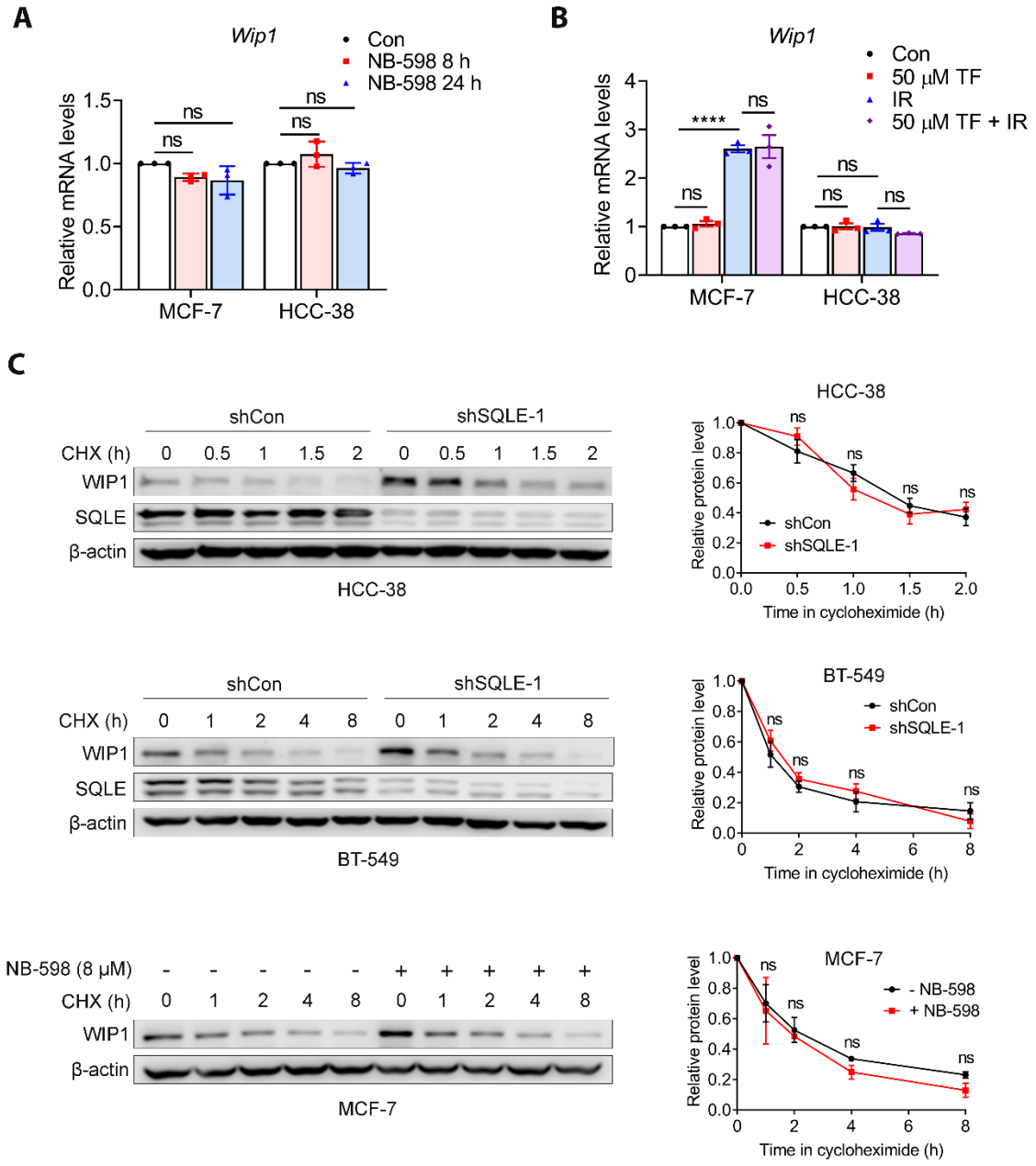

Supplemental Figure S13. SQLE inhibition had no effect on *WIP1* mRNA expression. A, SQLE inhibition by 8μM NB-598 had no effect on *WIP1* mRNA expression in MCF-7 and HCC-38 cells. **B,** SQLE inhibition did not alter IR-induced *WIP1* mRNA expression in cells with wild-type p53. *WIP1* transcription levels were measured 2 h post-2 Gy IR. All data in **A** and **B** are normalized with Con group. **C,** SQLE inhibition by shRNA or inhibitor did not affect WIP1 degradation. A similar WIP1 degradation rate was observed in cells with or without SQLE knockdown. WIP1 protein expression was quantified via Image J software. Data are presented as the mean ± SD. Statistical significance was evaluated with one-way ANOVA and Bonferroni's post-hoc test. ***, $P < 0.001$; ns, not significant.

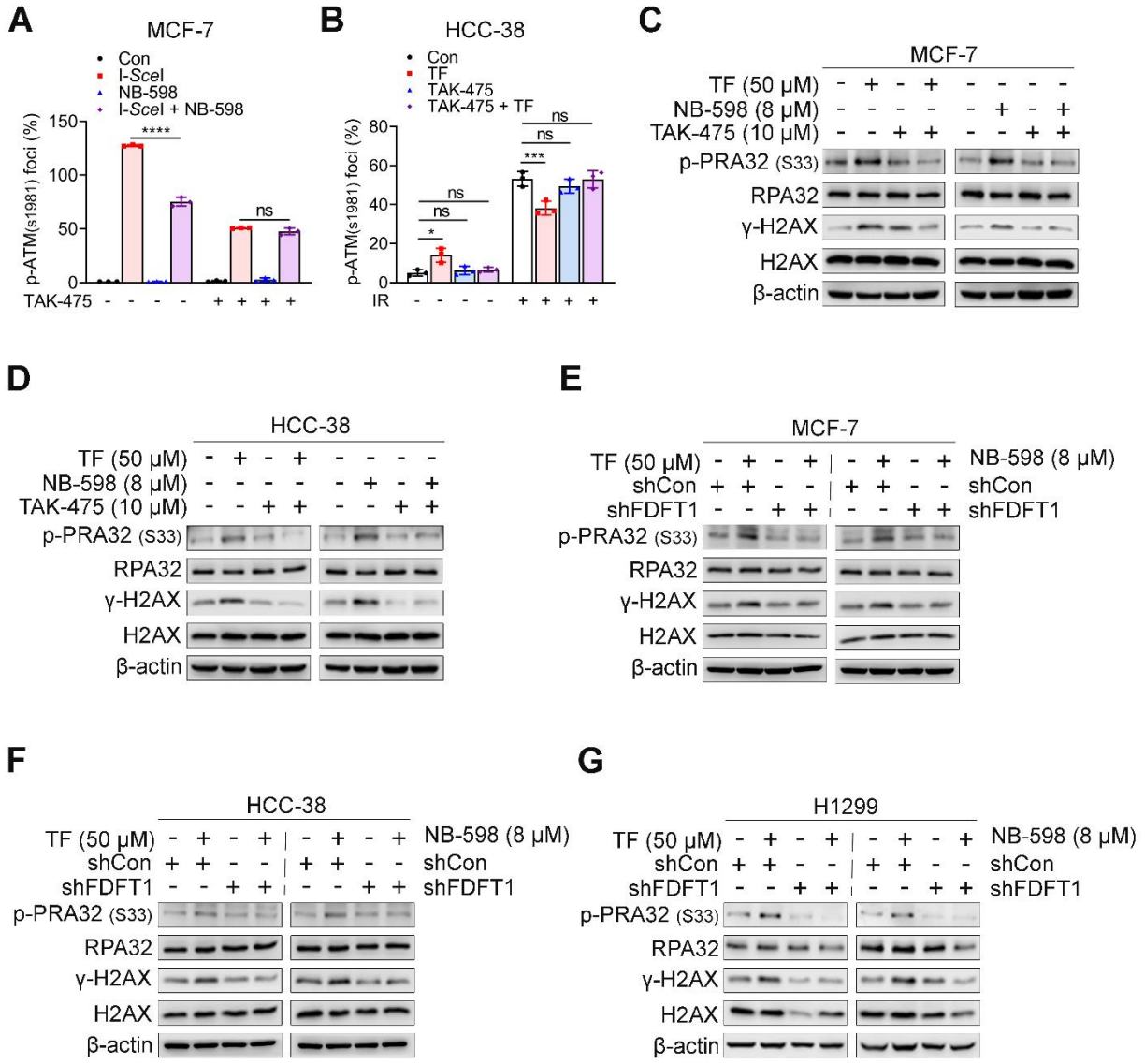

Supplemental Figures S14. SQLE inhibition-induced alterations in the WIP1-ATM axis and radiosensitivity were dependent on squalene. A, TAK-475 (10 μM) for 48 h abolished the SQLE inhibition (8 μM NB-598)-induced HR. All data are normalized with negative control. **B,** TAK-475 (10 μM) for 48 h abolished the SQLE inhibition (50 μM TF)-induced reduction in IR (2 Gy)-induced p-ATM (S1981) foci in HCC-38 cells. Data are presented as the mean ± SD. Statistical significance was evaluated with one-way (**B**) or two-way (**A**) ANOVA and Bonferroni's post-hoc test. *, $P < 0.05$; ***, $P < 0.001$; ****, $P < 0.0001$; ns, not significant. **C** and **D,** TAK-475 (10 μM) blocked SQLE inhibition-induced replication stress (RS) in MCF-7 and HCC-38 cells. **E-G,** Squalene depletion by FDFT1 downregulation eliminated SQLE inhibition-induced RS in BC (**E** and **F**) and lung cancer (**G**).

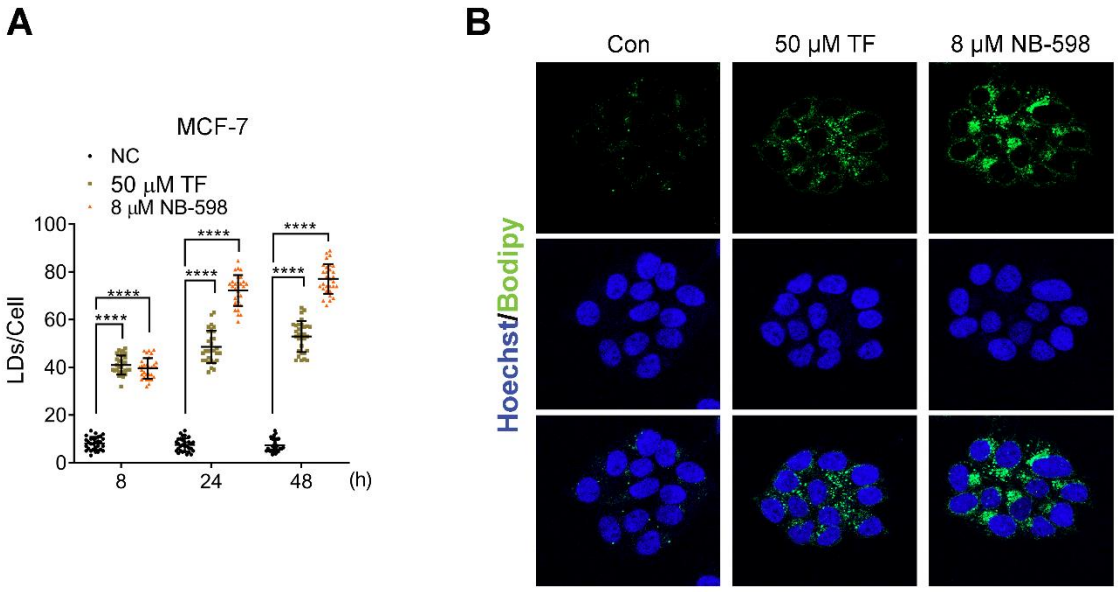

Supplemental Figure S15. SQLE inhibition increased LD formation. A, Qualification of LDs in MCF-7 cells treated with or without SQLE inhibitor TF (50 μM) or NB-598 (8 μM) at the indicated time points (mean ± SD, n = 30). **B,** Representative images of LDs in MCF-7 cells treated with SQLE inhibitors for 24 h. LD was stained with BODIPY 493/503 (green, upper panels), and the nuclei were stained with Hoechst 33342 (blue, middle panels) (magnification, 63× oil). Data are presented as the mean ± SD. Statistical significance was evaluated with two-way (**A**) and Bonferroni's post-hoc test. ****, $P < 0.0001$.

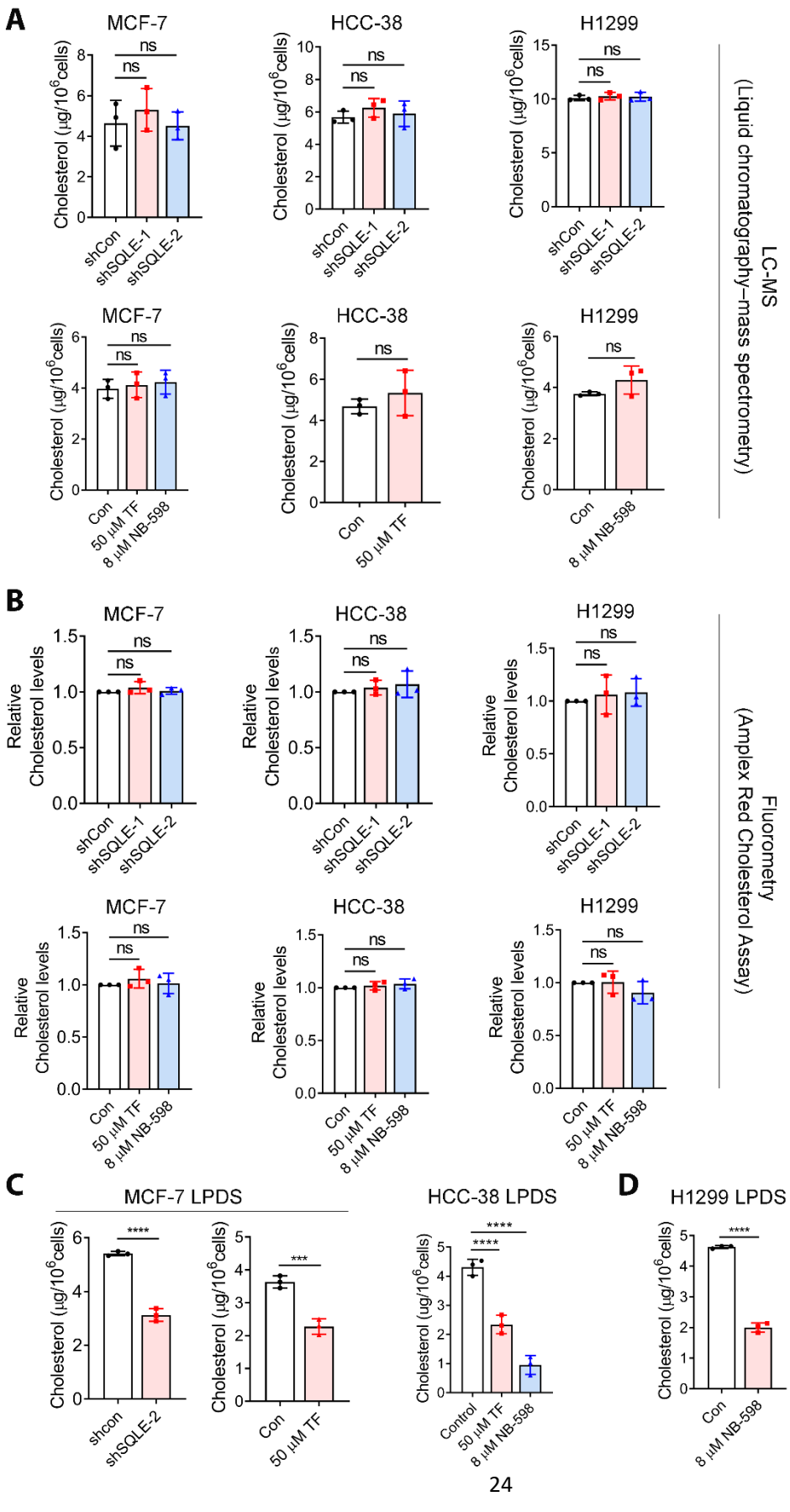
A
MCF-7
HCC-38
H1299
Cholesterol (μg/10^6cells)
ns
shCon
shSQLE-1
shSQLE-2
Con
50 μM TF
8 μM NB-598
LC-MS
(Liquid chromatography–mass spectrometry)
B
Relative Cholesterol levels
Fluorometry
(Amplex Red Cholesterol Assay)
C
MCF-7 LPDS
HCC-38 LPDS
shcon
Control
****
***
D
H1299 LPDS

Supplemental Figure S16. SQLE inhibition had no impact on cholesterol levels. A and **B,** SQLE inhibition by shRNA knockdown or inhibitors had no impact on cholesterol levels in BC and lung cancer cells, as detected by LC-MS (**A**) and the Amplex Red Cholesterol Assay (**B**). All data in **B** are normalized with Con or shCon group. **C,** SQLE inhibition decreased cholesterol levels in BC cells cultured in LPDS medium (LC-MS). **D,** SQLE inhibition decreased cholesterol levels in H1299 cell cultured in LPDS medium. Data are presented as the mean ± SD. Statistical significance was evaluated with one-way ANOVA and Bonferroni's post-hoc analysis for multiple comparisons. ***, $P < 0.001$; ****, $P < 0.0001$; ns, not significant.

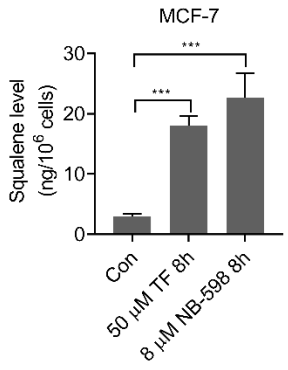

Supplemental Figure S17. SQLE inhibition led to the accumulation of squalene. SQLE inhibition with 50 μM TF or 8 μM NB-598 led to increased squalene levels eight hours after treatment. Data are presented as the mean ± SD. Statistical significance was evaluated with one-way ANOVA and Bonferroni's post-hoc test for multiple comparisons. ***, $P < 0.001$; ns, not significant.

References

1. Wan L, Liu T, Hong Z, Pan Y, Sizemore ST, Zhang J*, et al.* NEDD4 expression is associated with breast cancer progression and is predictive of a poor prognosis. Breast Cancer Res **2019**;21:148
2. Yang X, Pan Y, Qiu Z, Du Z, Zhang Y, Fa P*, et al.* RNF126 as a Biomarker of a Poor Prognosis in Invasive Breast Cancer and CHEK1 Inhibitor Efficacy in Breast Cancer Cells. Clinical cancer research : an official journal of the American Association for Cancer Research **2018**;24:1629-43
3. Zhang Y, Lai J, Du Z, Gao J, Yang S, Gorityala S*, et al.* Targeting radioresistant breast cancer cells by single agent CHK1 inhibitor via enhancing replication stress. Oncotarget **2016**
4. Wang Y, Deng O, Feng Z, Du Z, Xiong X, Lai J*, et al.* RNF126 promotes homologous recombination via regulation of E2F1-mediated BRCA1 expression. Oncogene **2016**;35:1363-72
5. Geng F, Cheng X, Wu X, Yoo JY, Cheng C, Guo JY*, et al.* Inhibition of SOAT1 Suppresses Glioblastoma Growth via Blocking SREBP-1-Mediated Lipogenesis. Clinical cancer research : an official journal of the American Association for Cancer Research **2016**;22:5337-48
6. Ray KJ, Sibson NR, Kiltie AE. Treatment of Breast and Prostate Cancer by Hypofractionated Radiotherapy: Potential Risks and Benefits. Clin Oncol (R Coll Radiol) **2015**;27:420-6
7. Klement RJ, Sonke JJ, Allgauer M, Andratschke N, Appold S, Belderbos J*, et al.* Estimation of the alpha/beta ratio of non-small cell lung cancer treated with stereotactic body radiotherapy. Radiotherapy and oncology : journal of the European Society for Therapeutic Radiology and Oncology **2020**;142:210-6